Research Article | Vol. 15, No. 3 / 1 Mar 2024 / Biomedical Optics Express 1682
Biomedical Optics EXPRESS

Photodynamic treatment of malignant melanoma with structured light: *in silico* Monte Carlo modeling

ALEXANDER DORONIN,[1,*] VLADISLAV V. YAKOVLEV,[2,3] AND VANDERLEI S. BAGNATO[3,4]

[1] *School of Engineering and Computer Science, Victoria University of Wellington, Wellington, 6140, New Zealand*
[2] *Department of Physics and Astronomy, Texas A&M University, College Station, Texas, USA*
[3] *Department of Biomedical Engineering, Texas A&M University, College Station, Texas, USA*
[4] *Institute of Physics, São Carlos, São Paulo University, Brazil*
[*] *alex.doronin@vuw.ac.nz*

Abstract: In this report, we propose a novel strategy for the photodynamic approach to the treatment of melanoma, aiming to mitigate the excessive absorption and consequent thermal effects. The cornerstone of this approach is an innovative structured illumination technique that optimizes light delivery to the tissue. The methodology of this *in silico* study involves the development of an optical model of human skin with the presence of melanoma and an accurate simulation technique of photon transport within the complex turbid scattering medium. To assess the effectiveness of our proposed strategy, we introduced a cost function reflecting the irradiated volume and optical radiation absorption within the target area/volume occupied by malformation. By utilizing the cost function, we refine the offset illumination parameters for a variety of target system parameters, ensuring increased efficiency of photodynamic therapy. Our computer simulation results introduce a promising new path towards improved photodynamic melanoma treatments, potentially leading to better therapeutic outcomes and reduced side effects. Further experimental validation is needed to confirm these theoretical advancements, which could contribute towards revolutionizing current melanoma photodynamic treatment methodologies.

© 2024 Optica Publishing Group under the terms of the Optica Open Access Publishing Agreement

1. Introduction

Melanoma is one of the most severe types of skin cancer, arising from the pigment-producing cells known as melanocytes. It is characterized by the uncontrolled growth of these cells, most commonly in the skin, but it can also develop in the eyes and, rarely, in internal organs. Melanoma is particularly dangerous due to its ability to spread to other parts of the body, a process known as metastasis, and it's often a challenging task to conventional cancer treatments [1]. The danger of melanoma lies not only in its aggressive nature but also in its increasing incidence. Over the past few decades, melanoma rates have been rising steadily worldwide. Despite representing only a small percentage of skin cancer cases, melanoma accounts for the majority of skin cancer deaths due to its high potential for spreading and resistance to treatment [2]. Australia and New Zealand, in particular, have the highest incidence rates of melanoma globally. This high incidence is likely due to the predominantly fair-skinned population, high levels of UV radiation, and outdoor lifestyle. Melanoma is the third most common cancer in Australia and the fourth most common in New Zealand. It represents a significant public health burden in these countries, both in terms of mortality and healthcare costs [3]. In the United States, melanoma is also a significant health concern. While the overall incidence rate is lower than in Australia and New Zealand, certain states with high levels of sun exposure, such as Florida and California, have higher incidence rates [4]. In 2023, it is estimated that 97,610 adults in the United States will be diagnosed with

#515962 https://doi.org/10.1364/BOE.515962
Journal © 2024 Received 14 Dec 2023; revised 6 Feb 2024; accepted 8 Feb 2024; published 15 Feb 2024

Biomedical Optics EXPRESS

invasive melanoma of the skin, while in 2020, approximately 324,635 people worldwide were diagnosed with melanoma. In 2020, an estimated 57,043 people worldwide died from it [5].

The treatment landscape for melanoma has expanded significantly over the past decades, evolving from surgery and chemotherapy to more advanced therapies such as immunotherapy, targeted therapy, radiation therapy, and photodynamic therapy [6]. Surgery is usually the first-line treatment for melanoma, especially in early-stage cases where the cancer has not spread beyond the skin. It involves the removal of the tumor along with some healthy tissue around it to ensure no cancer cells are left behind [6]. Nevertheless, assessing surgical margins often remains a challenging task for surgeons.

Photodynamic Therapy (PDT) is another treatment modality that has gained considerable interest in recent years. The principle of PDT lies in the administration of a photosensitizing agent which, upon light activation, induces a series of chemical reactions leading to the generation of reactive oxygen species (ROS). These ROS can cause cell death, destroy blood vessels supplying the tumor, and stimulate an immune response against the cancer cells [7,8]. PDT offers several advantages, including being a non-invasive procedure with fewer side effects. However, the effectiveness of PDT depends on various factors, such as the type and dose of the photosensitizing agent, the light source, and the tissue's properties with respect to its capacity to transmit enough light. Light absorption by melanin is considered as one of the most important limitations. Optimizing these factors is critical for improving PDT outcomes [9,10]. Despite the potential of PDT, its adoption in routine melanoma treatment is still limited. More research is needed to fully understand its long-term efficacy and safety profile. However, as our understanding of melanoma and its treatment continues to grow, there is hope that we can improve the prognosis for patients diagnosed with this aggressive form of cancer.

In this report, we specifically explore one crucial aspect of PDT for melanoma treatment: the influence of absorption by the melanoma cells resulting in overheating and insufficient photodynamic action response. Overheating and limited photodynamic action can lead to necrosis, an uncontrolled form of cell death that can instigate inflammation, potentially promoting tumor recurrence and spread [11]. When cells die from necrosis, their contents, including potentially harmful substances, are released into the surrounding tissue. This can trigger inflammation. In some cases, this inflammation can potentially promote tissue stimulated regeneration and, therefore, increase chances of tumor recurrence and spread/metastasis. The exact relationship between overheating, necrosis, inflammation, and cancer progression can be quite complex and can depend on a variety of factors, including the size, shape and depth of melanoma, the specific conditions illumination and many others. In order to provide the insight on those complexities, we investigate *in silico* the potential of so-called structured optical illumination on melanoma and the surrounding tissues. The term "structured light" by itself carries diverse interpretations across various fields, including optics, computer vision, and 3D scanning, where it may encompass differing concepts. Within the realm of Biomedical Optics, however, "structured light" assumes a distinct meaning, referring to the deliberate customization and manipulation of light across all its facets, including amplitude, phase, and polarization modulation [12]. In our investigation, the light source is intentionally deviated from the target melanoma site, aiming to reduce excessive light incidence on it without missing illumination of all the surroundings to produce efficient necrosis (see Fig. 1).

In this study, we utilize our recently introduced, open-source, power efficient Monte Carlo (MC) method developed *in house*: **Neu(t)ralMC** [13]. While the statistical nature of MC solutions introduces computational inefficiencies, it also enables efficient parallelization strategies [14–16]. These advances have enhanced handling of complex light-tissue interactions, leading to developments in computational efficiency, accurate tissue models, and novel applications in biomedical optics, such as spectra analysis, polarization, coherence properties, angular momentum of light, etc. [17–25]. Recently, the intersection of Biomedical Optics and Machine

Biomedical Optics EXPRESS

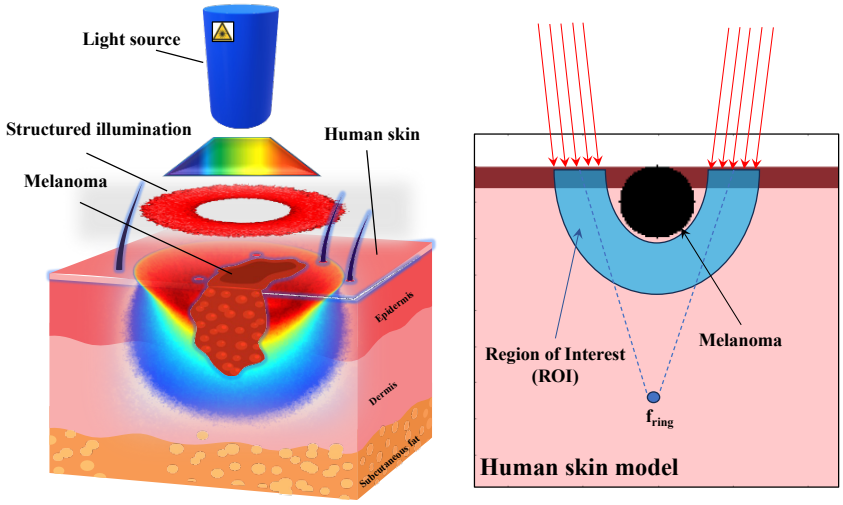

Fig. 1. Schematic representation of the structured illumination concept in Photodynamic Therapy for melanoma treatment is presented. We assess the light distribution as a ring incident on melanoma-affected tissue, focused towards a specific point within the scattering medium. Our investigation encompasses light deposition both within the melanoma and the surrounding tissue region of interest (ROI).

Learning (ML) has opened novel avenues for solving complex problems, enabling tasks like estimating chromophore concentrations from hyperspectral images, detecting cancerous tissues, and polarimetry [26,27].

We have developed further the mathematical representations of melanoma and surrounding tissue as distinct 3D volumetric regions with unique optical properties, thus capturing their differential interactions with the structured illumination. This approach enabled us to quantify and visualize the spatial distribution of light, especially within and around the malformation site. By introducing a tailored cost function, we are able to fine-tune the parameters of the offset illumination in order to cater for different target system parameters, effectively mitigating the tissue overheating for photodynamic therapy effectiveness.

The results from our MC simulations and subsequent analyses revealed that offset illumination could effectively deliver therapeutic light to surrounding tissues while limiting the exposure and potential thermal damage to the melanoma cells. The outcomes from these simulations provide an essential understanding of how to manipulate and optimize the offset illumination parameters to achieve the desired distribution of light, thereby improving the efficacy and safety of photodynamic therapy for melanoma. We believe that the insights derived from this numerical study have significant implications for the future development and optimization of targeted photo therapy strategies for melanoma treatment.

2. Light transport in melanoma-affected skin and offset illumination

In the framework of optical simulations, human skin is usually represented as a multi-layered (or multi-voxel) structure: the epidermis, the dermis, and the subcutaneous tissue. Briefly, each layer is characterized by specific values of absorption $\mu_a(\lambda)$ and scattering $\mu_s(\lambda)$ coefficients and anisotropy factor $g(\lambda)$ [28–30]. These parameters depend on the wavelength of the incident light and the specific composition of the skin layer. The outermost layer, the epidermis, contains melanocytes, which produce melanin, a pigment that absorbs and scatters ultraviolet and visible light. Greater melanin concentrations can lead to higher levels of light absorption and less

Biomedical Optics EXPRESS

transmission of light into deeper skin layers. Below the epidermis is the dermis, which contains structures such as collagen fibers, elastin, and blood vessels. Blood within the vessels contributes to the skin's optical properties through its absorption and scattering of light. The blood volume fraction, or the volume of blood relative to the total volume of the dermis, can influence the degree of light absorption. Additionally, the oxygen saturation level of the blood can alter the absorption spectrum, as oxygenated and deoxygenated hemoglobin have different absorption coefficients. Lastly, the subcutaneous layer, composed mostly of fat and connective tissue, also interacts with light in unique ways. The presence of blood vessels in this layer means that the blood volume fraction and oxygen saturation level can also affect the optical properties here. These variables play key roles in determining how light interacts with the skin, which is essential knowledge in fields such as dermatology, cosmetic science, phototherapy, and optical diagnostics with a number of models developed in the past accurately accounting for these complex variety of factors [18,29,31–34].

Melanoma, which originates from melanocytes, exhibits distinctive optical properties, primarily due to the overproduction of melanin. These properties can be quantitatively expressed in terms of absorption and scattering coefficients, as well as the anisotropy factor. The exact optical properties of melanoma can vary dramatically, depending on tumor type, such as dark and opaque melanomas, and the actual dynamics of the disease with the actual research being limited on this topic. For instance, it has been reported that the absorption coefficient of melanoma in the visible spectrum (400-700 [nm]) can range from 1 to 10 [mm^{-1}] [35], mainly due to the increased melanin content. In contrast, healthy skin typically has an absorption coefficient of approximately order of magnitude lower in the same spectral region. Typically, melanoma tissue exhibits a lower anisotropy factor compared to healthy skin, implying a less forward-peaked scattering phase function. In our simulation, we employed the Henyey–Greenstein (HG) phase function to model light transport within all layers. Specifically, at each scattering event, we determined the direction vector $\vec{\omega}_i'$ using the Henyey–Greenstein phase function, which was originally introduced into MC simulations by Prahl [32], building upon the work by Henyey and Greenstein [36]. More recently, an improvement of generation of accurate scattering phase functions using two terms has been proposed [37]. The anisotropy factor of melanoma tissue varies around 0.8, in contrast to approximately 0.9 for normal skin tissue [38]. The scattering coefficient of melanoma tissue also differs from that of normal skin, attributable to altered cellular and extracellular structures. Both lower and higher levels have been reported [35]. Nevertheless, it is important to point out that these values can significantly vary among patients and even within a single lesion due to the heterogeneous nature of melanoma [39–41].

In this study, our aim is not to establish the accurate optical properties of melanoma, which require careful experimentation and capture, but rather to establish a methodology for numerical assessment towards improved PDT treatments. Therefore, in order to provide a baseline for our study of the offset illumination, we focus exclusively on "dark" inhomogeneous melanomas. For this task, we have integrated the optical properties of biological tissues into a single voxelized model, i.e., the model is divided into small volumetric elements, each representing a voxel with assigned optical properties based on the composition and characteristics of the medium. Our model contains both healthy skin regions such as the epidermis, dermis, as well as embedded melanoma structure (see Fig. 1). We utilize the numerical procedure developed earlier, which employs precise chromophore concentrations and analytical expressions for calculating the optical properties of biological tissues, as described in [28,29]. These optical properties, essential for simulating light transport within melanoma-affected skin, are summarized in Table 1.

Our voxelized model incorporates essential parameters such as absorption, scattering, and anisotropy in order to to simulate the behavior of light within the tissue at various wavelengths. In order to study the influence of the offset illumination *in silico* the Radiative Transfer Equation (RTE) needs to be evaluated. The RTE can be challenging to solve, especially for complex

Biomedical Optics EXPRESS

Table 1. Optical properties and geometry of human skin with melanoma at selected wavelengths have been calculated using numerical procedure described in [28,29]: Anisotropy factors set to $g = 0.9$ for healthy tissues and $g = 0.8$ for melanoma regions. High volume fraction of melanin ($C_{mel} = 45\%$) has been set for melanoma region with the properties of the tissue-air interface defined as: $\mu_a = 0.0001$, $\mu_s = 0.1$, $g = 1.0$, and $n = 1.4$.

Tissue	600 [nm]		800 [nm]		Thickness [mm]
	$\mu_a, [mm^{-1}]$	$\mu_s, [mm^{-1}]$	$\mu_a, [mm^{-1}]$	$\mu_s, [mm^{-1}]$	
Epidermis	0.9292	31.6	0.4275	25.0	0.06
Dermis	0.0023	23.0	0.0022	14.1	2.0
Melanoma	13.9344	15.8	6.3910	12.5	$r_{mel} = 0.1$

inhomogeneous medium where optical properties change significantly. It has been previously demonstrated, that no general analytic solution exists for such tasks and stochastic MC methods have proved themselves as a gold standard, providing accurate solutions to RTE in complex, inhomogeneous media/geometry in the field of Biomedical Optical diagnostics. In the framework of this research we utilize our next generation online open-source power-efficient MC specifically created for the Apple M-family processors [42,43]. Our model has been recently enhanced with ML capabilities and is fully compatible with the input/output data structures of *MCXYZ.C* program introduced by Biomedical Optics pioneer S. Jacques [30].

A specific, structured illumination source function has been introduced to *Neu(t)ralMC*, is characterized by its unique light delivery pattern. In this approach, the photons do not originate from a singular point, but instead are launched from a defined shape, e.g. a ring pattern. This approach marks a significant departure from traditional optical treatment illumination techniques, where light is typically directed from a single source directly onto the treatment area. In our structured illumination setting, the amplitude control is exclusively considered with photons launching from various points along the ring, entering the scattering medium from multiple angles and positions. This multi-point and multi-angle approach inherently broadens the spatial distribution of light within the medium. Furthermore, photons are focused towards a specific point within the medium itself, enabling a targeted delivery of light while minimizing surface exposure. This is particularly advantageous in scenarios where the target lies deep within the tissue, as it reduces the likelihood of surface overheating and allows for a more concentrated treatment at the desired depth. In practice, for a photon packet its initial position $\mathbf{p}_0(x_0, y_0, z_0)$ and directional cosines $\omega_\mathbf{0}(s_x, s_y, s_z)$ located at a boundary interface ($z_0 = 0$) are characterized by:

$$
\begin{aligned}
&r_0 = r_{ring} + d_{ring} \cdot \sqrt{\xi_1} \quad \phi = 2.0 \cdot \pi \cdot \xi_2 \\
&x_0 = r_0 \cdot \cos(\phi) \quad y_0 = r_0 \cdot \sin(\phi) \\
&x_f = x_t - x_0 \quad y_f = y_t - y_0 \quad z_f = z_t \\
&s_x = x_f / \sqrt{x_f^2 + y_f^2 + z_f^2} \quad s_y = y_f / \sqrt{x_f^2 + y_f^2 + z_f^2} \quad s_z = \sqrt{1.0 + s_x^2 + s_y^2} \\
&\mathbf{p}_0 = \{x_0, y_0, z_0\} \quad \omega_\mathbf{0} = \{s_x, s_y, s_z\}
\end{aligned}
\tag{1}
$$

where r_0 corresponds to the randomly chosen radius within a ring of inner radius r_{ring} and thickness d_{ring}, $\xi_{1,2}$ are the two uniformly distributed random numbers between $[0, 1)$, $f_{ring}(x_t, y_t, z_t)$ is the target focal point located within a scattering medium. The procedure for a ring offset illumination focusing towards chosen point in the medium include two steps: assignment of a starting position within the ring and setting initial direction of each photon towards a specified point in the medium. Inner and outer radius define the radii of the ring, while target point represents the coordinates in the medium the photons are focused towards. The first random number is used to calculate the

Biomedical Optics EXPRESS

radius of the current photon within the ring. The $\sqrt{\xi_1}$ ensures a uniform distribution of photons within the ring. The second random number is used to calculate the angle ϕ of the photon on the ring in the x-y plane. The photon's initial position is calculated by using the radius and angle. The starting z-coordinate of the photon is a constant and corresponds to medium interface plane. Finally, the directional vector from the photon's starting position to the target point is calculated and normalized.

3. Evaluation and discussion

In our MC simulations, a key output parameter is the radially-resolved fluence rate distribution, denoted as $\Phi(r, z)$. This distribution, which depends on both radial and depth coordinates, represents the power delivered per unit area. Commonly referred to as irradiance, it was one of the first quantities introduced in Biomedical Optics [32] and represents the amount of light power delivered within a specific area and is typically expressed in units of watts per square centimeter (W/cm^2). Nowadays, the fluence rate assumes particular significance in various applications, including photodynamic therapy and photoacoustic imaging, where the precise amount of light delivered to the target tissue plays a crucial role in determining the therapy's effectiveness. Comprehensive insights into the basis of MC simulations for calculation fluence rate distributions are provided in details in [44–46].

Nevertheless, in PDT for melanoma the use of photosensitizing agents is involved, which are activated by light of a certain wavelength [47]. This activation causes the photosensitizing agents to produce reactive oxygen species that can destroy cancer cells. The specific wavelength of light used in PDT depends on the photosensitizing agent being used. Most photosensitizers are activated by light in the red or near-infrared wavelengths because these wavelengths can penetrate tissue more deeply than light of shorter wavelengths. For instance, a common photosensitizing agent used in PDT is porfimer sodium (Photofrin), which is activated by light of approximately 630 [nm], in the red part of the spectrum. Another photosensitizer, aminolevulinic acid (ALA), leads to the production of protoporphyrin IX in the tissue, which is activated by light of around 635-640 [nm]. In some experimental melanoma treatments, new photosensitizers are being explored, including ones that are activated by light in the near-infrared part of the spectrum (around 700-800 [nm]), which can penetrate even deeper into tissue.

We perform numerical simulations for selected wavelengths (630 and 800 [nm]) and define a multi-parametric cost function, denoted as $J(mel, ROI)$, which aims to minimize the fluence Φ_{mel} delivered to melanoma and maximize fluence Φ_{ROI} within our pre-defined region of interest (ROI) in the tissues:

$$J(mel, ROI) = \int_{V_1} S(\mathbf{u}) \frac{\Phi_{mel}(\mathbf{u})}{\Phi_{mel}^{baseline}(\mathbf{u})}^2 d\mathbf{u} - \int_{V_2} S(\mathbf{v}) \frac{\Phi_{ROI}(\mathbf{v})}{\Phi_{ROI}^{baseline}(\mathbf{v})}^2 d\mathbf{v} \tag{2}$$

In this equation, $S(\mathbf{u})$ and $S(\mathbf{v})$ correspond to the weighting functions that is used to prioritize parts of volume occupied by melanoma and our ROI, $\Phi_{mel}^{baseline}$ and $\Phi_{ROI}^{baseline}$ signify fluence rates delivered to melanoma and ROI using traditionally used uniform illumination approach. Our ROI targets the optimal treatment area aiming to encapsulate melanoma and is described using set notation as follows.

Firstly, we define $S(\mathbf{u},\mathbf{v})$ to represent the set of points in the hemisphere of the tissue region with a radius of $2r_{\text{mel}}$:

$$S(\mathbf{u},\mathbf{v}) = \left\{(x, y, z) \in \mathbb{R}^3 \mid x^2 + y^2 + z^2 \leq (2r_{\text{mel}})^2 \text{ and } z \geq 0\right\}$$

Secondly, $S(\mathbf{u})$ denotes the set of points within the hemisphere of melanoma of radius r_{mel}:

$$S(\mathbf{u}) = \left\{(x, y, z) \in \mathbb{R}^3 \mid x^2 + y^2 + z^2 \leq r_{\text{mel}}^2 \text{ and } z \geq 0\right\}$$

Biomedical Optics EXPRESS

Finally, the set of points representing the ROI is obtained by subtracting the melanoma region from the total tissue region, is:

$$S(\mathbf{v}) = S(\mathbf{u},\mathbf{v}) \setminus S(\mathbf{u})$$

Our *in house* parallel computing-accelerated MC model can effectively deal with the problem of optimization and able to generate a large amount of data that represents the photon transport in the medium within minutes. We use use this data to compute the fluence within target regions and find the best possible configuration using Algorithm 1. We focus on three essential parameters by normalizing their ranges using the melanoma radius r_{mel} for effective dimensionless representation. The first parameter, is the ring focus which fluctuates in a range of $2-10$ of r_{mel}.

Algorithm 1. Optimize light delivery using focused offset illumination

```
procedure OptimizeDelivery(configurations, regions)
    best_cost ← ∞
    best_params ← null
    for each config in configurations do          ▷ Iterate over possible configurations
        photon ← SetupFocusedRingIllumination(config)          ▷ See Equation 1
        fluence ← MonteCarloSimulation(config)          ▷ Simulate photon transport
        cost ← CostFunction(fluence, regions)          ▷ See Equation 2
        if cost < best_cost then          ▷ Update if current configuration is better
            best_cost ← cost
            best_params ← config
        end if
    end for
    return best_params
end procedure
```

The inner ring radius, signifies the foundational structure of the ring, spanning a range of $1-5$ of r_{mel}. Augmenting this, the ring thickness establishes the expanse of the ring, inherently defining its external boundary. Also ranging from $1-5$, this parameter enables adjustments to the ring's bulk and reach. The increments are performed in steps of $1/10$ r_{mel} collectively creating a search space consisting of 136, 161 candidate configurations. Computer modeling has been performed for 10^6 of photon packets using Apple M2 processors with each simulation completing nearly real-time, in a matter of just a few seconds (detailed performance considerations are presented in [13]).

The visualization of our MC-generated search space is presented in Fig. 2. The target is to optimize the cost function (see Eq. (2)), which involves adjusting the parameters of the light delivery system in a manner that the actual fluence rate aligns as closely as possible with the desired fluence rates throughout the target volumes. The presented cost function is a variant of the relative difference squared error function, weighted by the baseline (uniform) illumination simulations output. The best parameters are updated whenever a lower cost is found. Figure 3 provides a visual representation of the computed cost functions for two specific, disparate wavelengths. In this figure, the ring focus, a central parameter in our model, is set to a designated value and normalized with respect to the melanoma radius ($f_{ring} = 3 \times r_{mel}$). For each chosen wavelength, the figure delineates the variations of the cost function in relation to adjustments in both the inner ring radius and ring thickness parameters. Following the objective to methodically optimize the configuration of the light delivery system, this computation aims to achieve a fluence rate distribution within the targeted volumes that adheres as closely as possible to the desired fluence.

Following the extensive computations performed in our study, we have successfully identified trends that guide us towards the optimal configuration of the light delivery system for photodynamic

Biomedical Optics EXPRESS

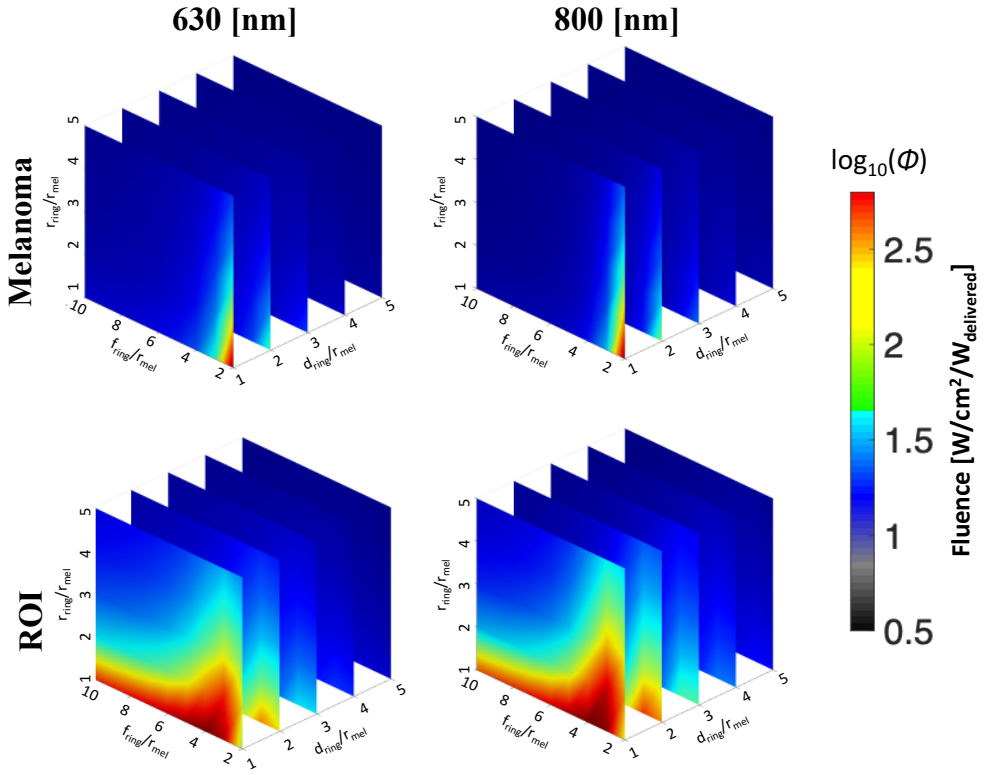

Fig. 2. Fluence rate distributions for two selected wavelengths, showcasing the parameters space, cross-sections and the influence of varying offset illumination parameters on Φ_{ROI} and Φ_{mel}. Parameters are normalized with respect to the melanoma radius, r_{mel}. The figure presents the effects of ring focus, inner ring radius, and ring thickness on light delivery within a target volume.

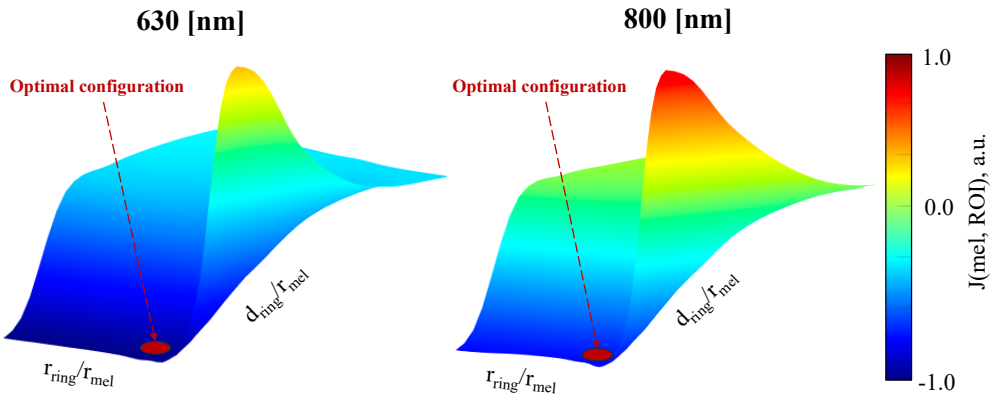

Fig. 3. Example of calculated cost function, as defined in Eq. (2), evaluated for two distinct wavelengths. In this figure, the ring focus is set to a specific value ($f_{ring} = 3 \times r_{ring}$), which is a pivotal parameter in our model, normalized with respect to the melanoma radius r_{mel}.

Biomedical Optics EXPRESS

therapy. For both 600 [nm] and 800 [nm] wavelengths, our results align with the following parameter relationships, which have been tailored based on the melanoma radius r_{mel}. Specifically, the optimal r_{inner} is found to be $1.2r_{\text{mel}} \pm 0.2r_{\text{mel}}$. This adjustment in the inner ring radius allows for precise targeting of melanoma-affected tissue, ensuring the effective delivery of light. Moreover, the ideal d_{ring} is set at $1.5r_{\text{mel}} \pm 0.5r_{\text{mel}}$, a configuration that enables optimal fluence delivery to the melanoma surrounding area while minimizing the risk of overheating the melanoma itself. Additionally, for precise and effective light delivery, the optimal f_{ring} should be set within the range of $3r_{\text{mel}}$ to $5r_{\text{mel}}$. This range has been identified as effective for both the 600 [nm] and 800 [nm] wavelengths under investigation, highlighting its critical role in our model. Moreover, the use of an 800 [nm] wavelength was found to be more effective, showing approximately a 20% increase in terms of light delivery to the targeted ROI. This higher efficiency at 800 [nm] is likely attributable to the reduced scattering and absorption at this longer wavelength, which allows the light to penetrate deeper into the tissue. This significant finding paves the way for the potential trials of modern photosensitizer agents that are specifically activated by light at near-infrared. Utilizing such photosensitizers in conjunction with our optimized light delivery system could enable more effective and targeted photodynamic therapy treatments, offering promising prospects for improved patient outcomes.

Figure 4 provides a comparison between traditional, uniformly lit PDT and the proposed novel offset illumination strategy for two distinct wavelengths: 600 [nm] and 800 [nm]. The parameters of the ring illumination system have been determined through our optimization scheme. This figure vividly illustrates the photon distribution within the tissue and underscores the evident advantages of the offset illumination approach. Notably, the offset strategy consistently yields a more focused and efficient light deposition to the melanoma-affected area. This targeted approach reduces the risk of melanoma overheating, which is a notable limitation of traditional uniformly lit PDT. Therefore, particularly when utilizing the 800 [nm], the offset illumination strategy emerges as a promising avenue for enhancing the effectiveness of PDT. The light distribution as it displayed in the first row of images in Fig. 4 allows identification of the necessary exposure time that will achieve an adequate light dose above the threshold for necrosis. This shell of necrotic region will isolate the melanoma. By restricting the necrotic region, it is possible to eliminate the tumor due to the lack of nutrients and/or by starvation.

Nevertheless, It is important to note that the work presented here is an *in silico* study exploring a novel modality of light delivery in PDT. As such, the findings, while promising, are theoretical in nature and are based on computational simulations. Rigorous experimental validation is essential to confirm the feasibility and effectiveness of this proposed offset illumination strategy. Future work should include *in vitro* and *in vivo* studies to capture the actual properties of melanomas, validate computational predictions made here, and to assess the practicality, safety, and efficacy of this new approach to light delivery in PDT applications. On the other hand, this study adopts a brute-force approach in its algorithm, wherein all possible configurations within the parameter space are exhaustively tested, a process that leaves room for further improvement.

For future, extensive parameter space searches such as different skin and skin cancer types, non-uniformly shaped melanomas, etc., employing a more efficient optimization strategy (e.g. ML-based) are warranted. One alternative could involve the iterative adjustment of the light delivery parameters, paired with corresponding evaluations of the cost function. In this context, numerical optimization techniques, such as gradient descent or genetic algorithms, could be employed to systematically identify the targeted and personalized light delivery strategy. This refined approach, as a part of our future work, would aim to achieve the optimal light delivery within the target volume more efficiently, thereby reducing both the computational load and the time necessary for computations.

Biomedical Optics EXPRESS

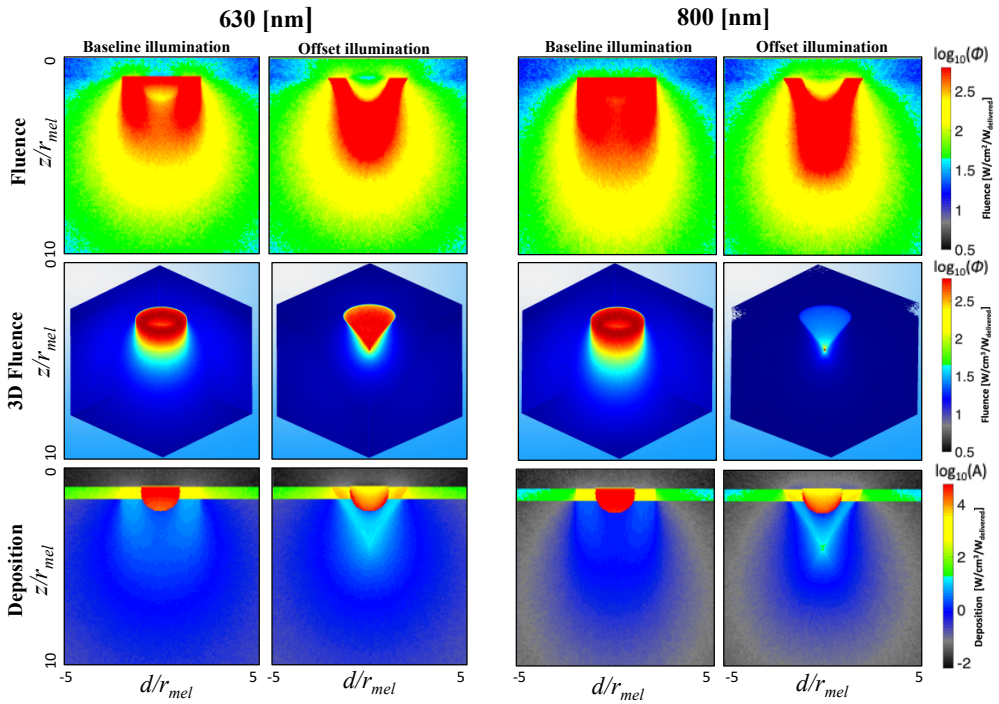

Fig. 4. Comparison of traditional and offset illumination strategies in PDT applications. In the proposed offset illumination approach, evaluated at two distinct wavelengths, light delivery is optimized to minimize damage to the melanoma region while simultaneously enhancing the fluence rate/deposition within the target ROI.

4. Conclusions

In this study, we introduced a novel approach for photodynamic melanoma treatment, specifically designed to alleviate the problem of overheating in melanoma cells, often associated with traditional methods. This strategy is anchored on an innovative structured illumination technique, offering optimized light delivery to the tissue. Our approach entailed the creation of detailed numerical and optical models, enabling precise simulation of light transport in complex turbid scattering media. Notably, our model incorporated a detailed optical depiction of melanoma-affected skin, accounting for the differing optical properties of various skin layers and melanoma cells. To evaluate the efficiency of our strategy, we formulated a cost function reflecting the irradiated volume and absorption of optical radiation within the target area. This cost function, when optimized, facilitated the fine-tuning of offset illumination parameters, thereby ensuring a more efficient photodynamic therapy with minimized thermal production.

Our pilot results point towards a promising route for improving photodynamic melanoma treatments, potentially yielding enhanced therapeutic outcomes and reduced adverse effects. However, these theoretical advancements require further experimental validation. As we move forward with our research, we plan to delve into optical experimentation methods and technologies for creating the desired illumination patterns. These techniques may involve the use of spatial light modulators (SLMs), diffractive optical elements (DOEs), beam shaping optics, and other tools for shaping the intensity of light beams [12]. Looking ahead, we acknowledge that there is significant potential for further development and expansion of our technique. One natural progression involves exploring polarization, phase and other control as integral components of

Biomedical Optics EXPRESS

our approach. Building upon our previous contributions in this area [20], we plan to extend our methodology to incorporate these additional degrees of freedom in light manipulation for PDT.

Once confirmed, these findings could potentially revolutionize current methodologies in melanoma photodynamic treatment, paving the way for safer and more effective interventions. With a precise knowledge of a lesion, which can be obtained independently through several imaging modalities, a highly personalized treatment plan can be developed with a follow-up monitoring and treatment.

Funding. Royal Society Te Apārangi (E3929); Air Force Office of Scientific Research (FA9550-20-1-0366, FA9550-20-1-0367); National Institutes of Health (1R01GM127696, 1R21CA269099, 1R21GM142107); U.S. Food and Drug Administration (80ARC023CA002E); Cancer Prevention and Research Institute of Texas (RR220054); Chancellor's Research Initiative; Texas Governor's University Research Initiative grant program.

Acknowledgments. VSB acknowledges support provided by the Chancellor's Research Initiative and the Texas Governor's University Research Initiative grant program.

Disclosures. The authors declare no conflicts of interest

Data availability. Data and code underlying the results presented in this paper are immediately available from [42].

References

1. D. Schadendorf, A. van Akkooi, C. Berking, *et al.*, "Melanoma," The Lancet **392**(10151), 971–984 (2018).
2. G. P. Guy, C. C. Thomas, T. D. Thompson, *et al.*, "Vital signs: Melanoma incidence and mortality trends and projections — United States, 1982–2030," Morbidity and Mortality Weekly Report **64**(21), 591–596 (2015).
3. F. Erdmann, J. Lortet-Tieulent, J. Schüz, *et al.*, "International trends in the incidence of malignant melanoma 1953–2008—are recent generations at higher or lower risk?" Int. J. Cancer **132**(2), 385–400 (2013).
4. R. L. Siegel, K. D. Miller, and A. Jemal, "Cancer statistics, 2020," CA A Cancer J. Clinicians **70**(1), 7–30 (2020).
5. "Melanoma: Statistics," Cancer Net (2023).
6. B. Domingues, J. M. Lopes, P. Soares, *et al.*, "Melanoma treatment in review," Immuno Targets Ther. **7**, 35–49 (2018).
7. P. Agostinis, K. Berg, K. A. Cengel, *et al.*, "Photodynamic therapy of cancer: an update," CA A Cancer J. Clinicians **61**(4), 250–281 (2011).
8. T. C. Pham, V. N. Nguyen, Y. Choi, *et al.*, "Recent strategies to develop innovative photosensitizers for enhanced photodynamic therapy," Chemical reviews (2021).
9. J. F. Algorri, M. Ochoa, P. Roldán-Varona, *et al.*, "Light technology for efficient and effective photodynamic therapy: a critical review," Cancers **13**(14), 3484 (2021).
10. P. Mróz, A. Yaroslavsky, G. B. Kharkwal, *et al.*, "Cell death pathways in photodynamic therapy of cancer," Cancers **3**(2), 2516–2539 (2011).
11. P. B. Elming, B. S. Sørensen, A. L. Oei, *et al.*, "Hyperthermia: The optimal treatment to overcome radiation resistant hypoxia," Cancers **11**(1), 60 (2019).
12. A. Forbes, "Structured light: Tailored for purpose," Opt. Photonics News **31**(6), 24–31 (2020).
13. A. Clennell, V. Nguyen, V. S. Yakovlev, *et al.*, "Neu(t)ralmc: energy-efficient open source Monte Carlo algorithm for assessing photon transport in turbid media," Opt. Express **31**(19), 30921–30931 (2023).
14. A. Doronin and I. V. Meglinski, "Peer-to-peer Monte Carlo simulation of photon migration in topical applications of biomedical optics," J. Biomed. Opt. **17**(9), 0905041 (2012).
15. I. V. Meglinski and A. Doronin, "Online Monte Carlo for biomedical optics," SPIE Newsroom (2011).
16. I. V. Meglinski and A. Doronin, "Monte carlo modeling of photon migration for the needs of biomedical optics and biophotonics," (2013).
17. A. Doronin, A. J. Radosevich, V. Backman, *et al.*, "Two electric field Monte Carlo models of coherent backscattering of polarized light," J. Opt. Soc. Am. A **31**(11), 2394–2400 (2014).
18. G. I. Petrov, A. Doronin, H. T. Whelan, *et al.*, "Human tissue color as viewed in high dynamic range optical spectral transmission measurements," Biomed. Opt. Express **3**(9), 2154–2161 (2012).
19. A. Doronin, C. M. Macdonald, and I. V. Meglinski, "Propagation of coherent polarized light in turbid highly scattering medium," J. Biomed. Opt. **19**(2), 025005 (2014).
20. A. Doronin, N. Vera, J. P. Staforelli, *et al.*, "Propagation of cylindrical vector laser beams in turbid tissue-like scattering media," Photonics **6**, 56 (2019).
21. A. Doronin, I. Fine, and I. V. Meglinski, "Assessment of the calibration curve for transmittance pulse-oximetry," Laser Phys. **21**(11), 1972–1977 (2011).
22. A. Doronin, L. Tchvialeva, I. Markhvida, *et al.*, "Backscattering of linearly polarized light from turbid tissue-like scattering medium with rough surface," J. Biomed. Opt. **21**(7), 071117 (2016).
23. I. V. Meglinski, C. M. Macdonald, A. Doronin, *et al.*, "Screening cancer aggressiveness by using circularly polarized light," OSA Technical Digest (2013).
24. B. H. Hokr, J. N. Bixler, G. Elpers, *et al.*, "Modeling focusing gaussian beams in a turbid medium with Monte Carlo simulations," Opt. Express **23**(7), 8699–8705 (2015).

Biomedical Optics EXPRESS

25. Z. Di, B. H. Hokr, H. Cai, *et al.*, "Spatially offset raman microspectroscopy of highly scattering tissue: theory and experiment," J. Mod. Opt. **62**(2), 97–101 (2015).
26. A. Doronin and I. V. Meglinski, "The application of a unified Monte Carlo model in the training of artificial neural networks for the purpose of real-time in-vivo sensing of tissue optical properties," in *Defense + Commercial Sensing*, (2019).
27. D. Robinson, K. Hoong, W. Kleijn, *et al.*, "Polarimetric imaging for cervical pre-cancer screening aided by machine learning: ex vivo studies," J. Biomed. Opt. **28**(10), 102904 (2023).
28. S. L. Jacques, "Optical properties of biological tissues: a review," Phys. Med. Biol. **58**(11), R37–R61 (2013).
29. I. V. Meglinski, A. Doronin, A. N. Bashkatov, *et al.*, "Dermal component–based optical modeling of skin translucency: Impact on skin color," in *Computational Biophysics of the Skin* (Pan Stanford, 2014), Chap. 2.
30. "mcxyz.c: A Monte Carlo model of light transport in 3d turbid media," https://omlc.org/software/mc/mcxyz/index.html. Accessed: 2023-05-03.
31. A. N. Bashkatov, E. A. Genina, V. I. Kochubey, *et al.*, "Optical properties of human skin, subcutaneous and mucous tissues in the wavelength range from 400 to 2000 nm," J. Phys. D: Appl. Phys. **38**(15), 2543–2555 (2005).
32. S. L. Jacques, "History of Monte Carlo modeling of light transport in tissues using mcml.c," J. Biomed. Opt. **27**(08), 083002 (2022).
33. I. V. Meglinski and S. J. Matcher, "Computer simulation of the skin reflectance spectra," Comput. Methods Programs Bioomed. **70**(2), 179–186 (2003).
34. I. V. Meglinski and S. J. Matcher, "Quantitative assessment of skin layers absorption and skin reflectance spectra simulation in the visible and near-infrared spectral regions," Physiol. Measurement **23**(4), 741–753 (2002).
35. V. V. Tuchin, "Tissue optics: Light scattering methods and instruments for medical diagnosis," SPIE (2000).
36. L. C. Henyey and J. L. Greenstein, "Diffuse radiation in the galaxy," The Astrophys. J. **93**, 70–83 (1941).
37. S. L. Jacques and N. J. Mccormick, "Two-term scattering phase function for photon transport to model subdiffuse reflectance in superficial tissues," Biomed. Opt. Express **14**(2), 751–770 (2023).
38. G. Zonios, J. Bykowski, and N. Kollias, "Skin melanin, hemoglobin, and light scattering properties can be quantitatively assessed in vivo using diffuse reflectance spectroscopy," J. Invest. Dermatol. **117**(6), 1452–1457 (2001).
39. M. A. L. M. Boone, M Suppa, F Dhaenens, *et al.*, "In vivo assessment of optical properties of melanocytic skin lesions and differentiation of melanoma from non-malignant lesions by high-definition optical coherence tomography," Arch. Dermatol. Res. **308**(1), 7–20 (2016).
40. A. Garcia-Uribe, E. B. Smith, J. Zou, *et al.*, "In-vivo characterization of optical properties of pigmented skin lesions including melanoma using oblique incidence diffuse reflectance spectrometry," J. Biomed. Opt. **16**(2), 020501 (2011).
41. G. Zonios, A. Dimou, M. Carrara, *et al.*, "In vivo optical properties of melanocytic skin lesions: Common nevi, dysplastic nevi and malignant melanoma," Photochem. Photobiol. **86**(1), 236–240 (2010).
42. A. Doronin,"Monte Carlo models and Code," Github, 2024, https://github.com/aledoronin/.
43. "Cloud based Monte Carlo tool for photon transport," https://www.lighttransport.net (2024).
44. L. V. Wang, S. L. Jacques, and L. Zheng, "MCML–Monte Carlo modeling of light transport in multi-layered tissues," Comput. Methods programs Biomed. **47**(2), 131–146 (1995).
45. L. V. Wang and S. L. Jacques, "Monte carlo modeling of light transport in multi-layered tissues in standard c," University of Texas M. D. Anderson Cancer Center (1992).
46. A. Doronin, "The unified Monte Carlo model of photon migration in scattering tissue-like media for the needs of biomedical optics," University of Otago (2014).
47. R. Baskaran, J. Lee, and S.-G. Yang, "Clinical development of photodynamic agents and therapeutic applications," Biomater. Res. **22**(1), 25 (2018).